MNRAS **000**, 000–000 (0000) Preprint 28 March 2018 Compiled using MNRAS LATEX style file v3.0

Lyman-α photons through rotating outflows

Maria Camila Remolina-Gutiérrez[1] ⋆ & Jaime E. Forero-Romero [1] †
[1] *Departamento de Física, Universidad de los Andes, Cra. 1 No. 18A-10 Edificio Ip, CP 111711, Bogotá, Colombia*

28 March 2018

ABSTRACT
Outflows and rotation are two ubiquitous kinematic features in the gas kinematics of galaxies. Here we perform Monte Carlo radiative transfer simulations of outflowing gas with additional solid body rotation to understand how these kinematic features impact the morphology of the Lyman-α emission line. We find three important consequences of rotation. First, it increases the detected flux at the line's center in comparison with the non-rotational case, second it produces a line broadening and third it introduces a dependency with the viewing angle. We also develp a semi-analytic model that modifies the spectra of pure outflow simulations that manages to reproduce the main features of the Monte Carlo simulations. As an application to observational data we constraint the rotation parameters of a set of observed LAE emission spectra.

Key words: galaxies: dwarf — radiative transfer — Methods: numerical

1 INTRODUCTION

The interpretation of the Lyman-α emission in galaxies is key to understand their evolutionary processes, specially in star-forming, low-dust galaxies (Partridge & Peebles 1967). Recent improvements in instrumentation have revolutionized the kind of studies that can be performed on Lyman-α emitting galaxies (LAEs.) For instance, it is now possible to infer detailed kinematic maps for nearby galaxies. The study of these maps would allow us to build data-driven models to interpret the Lyα spectra of unresolved galaxies, helping us to constrain the physical conditions of the interstellar medium (ISM) processing the Lyα radiation.

For instances, dwarf galaxies show signs of coherent rotation (Swaters et al. 2009). Some of them are expected to have high neutral gas contents and thus show Lyα emission with rotation imprints (**???**) Some Compact Dwarf Galaxies actually show gas kinematics that range from pure rotation to high velocity dispersion without a clear rotation pattern. (Cairós et al. 2015; Cairós & González-Pérez 2017)

The case for outflows as traced in the Lyα line is much bettwe stablished. There are abundance cases Lyα line profiles with a single peak redwards from the line's center. In other cases there is a double peak but the peak on the red side is stronger (e.g. **???**). This has been readily explained as the consequence of multiple Lyα photon scatterings through an homogeneous outflowing shell of neutral Hydrogen (**?**Orsi et al. 2012; **?**; **?**).

Here we present for the first time a study of the joint effects of galaxy outflows and rotation, two of the three major kinematic components expected in LAEs. We study a simplified geometrical configuration corresponding to a spherical gas cloud with symmetrical radial outflows and a rotation profile corresponding to a solid body. We base our modeling on a Monte-Carlo radiative transfer code called CLARA (Code for Lyman Alpha Radiation Analysis) presented for the first time by Forero-Romero et al. (2011).

Besides modeling the impact of joint rotation and outflows, we also check to what extent the analytical model presented by Garavito-Camargo et al. (2014) to explain the effects of rotation can also be applied in our case. We show how solid body rotation effects can be modelled by postprocessing the results of outflow only simulation.

in the results of other radiative transfer model in the case of large optical depths. In this case it is a good approximation to Doppler boost the results of the model without rotation.

The structure of the paper is the following. We introduce first our theoretical tools and assumptions in Section 2. We continue in Section 3 with the results from the Monte-Carlo simulation, the comparison against the semi-analytical approximation which we use to make a thorough exploration of the effect of rotation. In Section 4 we discuss our results and their possible implications for observational analysis to finally present our conclusions in Section 5.

2 THEORETICAL MODELS

The Monte Carlo code we use (CLARA) follows the propagation of individual photons through a neutral Hydrogen

⋆ mc.remolina197@uniandes.edu.co
† je.forero@uniandes.edu.co

$\tau_{\rm H}$	$V_{\rm rot}$ (km s^{-1})	$V_{\rm out}$ (km s^{-1})
$\{10^5, 10^6, 10^7\}$	{0, 50, 100}	{5, 25, 50}

Table 1. Parameters' Values. List of values that were used to construct the radiative transfer models. Values in braces for a row indicate that all possible combinations in of $\tau_{\rm H}$, $V_{\rm rot}$ and $V_{\rm out}$ are used.

medium characterized by its temperature, velocity field and global optical depth. The code assumes an homogeneous density throughout the simulated volume. In the current implementation we neglect the influence of dust. Our basic model is an spherical distribution of neutral hydrogen, an approximation commonly used in the literature, as it explains a wide variety of observational features (Ahn et al. 2003; Verhamme et al. 2006; Dijkstra et al. 2006).

The velocity field we use captures both outflows and rotation. Outflows are described by a Hubble-like radial velocity profile with the velocity magnitude increasing linearly with the radial coordinate; the outflows model is fully characterized by $v_{\rm out}$, the velocity at the sphere's surface. Rotation follows a solid body rotation profile, which is fully characterized by $V_{\rm rot}$, the linear velocity at the sphere's surface.

The total velocity field corresponds to the superposition of rotation and outflows. The cartesian components take the following form:

$$v_x = \frac{x}{R} V_{\rm out} - \frac{y}{R} V_{\rm rot}, \quad (1)$$

$$v_y = \frac{y}{R} V_{\rm out} + \frac{x}{R} V_{\rm rot}, \quad (2)$$

$$v_z = \frac{z}{R} V_{\rm out}, \quad (3)$$

where x, y and z are the cartesian position coordinates with the origin at the sphere's center, R is the radius of the sphere and the direction of the angular velocity vector corresponds to the $\hat{k}$ unit vector.

For each model setup we follow 10^5 individual photons generated at the center of the sphere at the Lyα line's center as they propagate through the volume and finally scape. We store the final frequency and propagation direction for each photon at its last scattering.

In Table 1 we list the combination of $\tau_{\rm H}$, $V_{\rm rot}$ and $V_{\rm rot}$ values used in this paper. The range of values have some overlap with the expectations from a dwarf galaxy with a total neutral hydrogen mass of 10^8-10^9 $M_\odot$. We run a total of 27 different models.

Garavito-Camargo et al. (2014) presented an analytical model that accounts for the effects of pure rotation on the Lyα line morphology. The basic assumption of their analytical model is that each differential surface element on the sphere Doppler shifts the photons that it emits. In this paper we introduce this ansatz by post-processing the results of the outflows simulations without rotation. The frequency of each photon is Doppler shifted as follows

$$x' = x + \frac{\vec{V}_{\rm rot} \cdot \hat{k}}{v_{\rm th}} \quad (4)$$

where x' is the photon's new frequency, x is the photon's frequency after being procesed by the outflow, $v_{\rm rot}$ is the rotational velocity at the point of escape of the photon, $\hat{k}$ is the photon's direction of propagation and $v_{\rm th}$ is the thermal velocity of the sphere.

This allows us to produce new Lyα spectra and compare them with the full radiative transfer solution including both outflows and rotation.

3 RESULTS

3.1 Qualitative Trends

Figure 1 summarizes the most important trends of our simulations. The six panels correspond to $\tau = 10^6$ and a viewing angle of $\theta = 90^{\rm deg}$, that is perpendicular to the rotation axis of the galaxy. In every panel the thin black line corresponds to the pure outflow solution (i.e. without rotation). From top to bottom we see the effect of increasing the outflow velocity, which is the expected increasing asymmetry towards the red peak.

The thick black line corresponds to the solution that includes both outflows and rotation. Comparing the left and right columns (lower versus higher rotational velocity) we can see two immediate effects. First, the line broadens and second, the intensity at the line's center increases.

Finally, the thick gray line correspods to the pure outflow solution with the Doppler boost added to model rotation's influence. In all cases the Doppler boost does a good job at capturing the broad morphological features introduced by rotation: the angle dependence, the broadening and the intensity increase at the line's center.

In Figure **??** we show the same results as in Figure 1 but for a viewing angle of $\theta = 90^{\rm deg}$, that is parallel to the rotation axis. In this case we see that the effect of rotation is very hard to see. As **??** showed, pure rotation introduces a strong dependence with viewing angle, a trend that we find also holds for rotation mixed with ouflows.

3.2 Quantitative trends

After finding the qualitative influence of the different parameters.

We evaluate the effects of increasing outflows velocity at fixed values for the optical depth and rotational velocity. Figure A2 summarizes its behavior (for a largest range see Figure A4). All plots correspond to the same rotation velocity of $\rm V_{rot} = 50 km\ s^{-1}$, rows have constant optical depth and columns have constant outflows velocity.

Figure 1 displays this Doppler shift for six different configurations with a fixed optical depth $\tau_{\rm H}$. In each cell of the grid there is a Lyα spectrum for a galaxy with only outflows and two Lyα spectra for the galaxy with outflows and rotation: one obtained from the radiative transfer simulation and the other obtained from the Doppler shifting of the non-rotating galaxy.

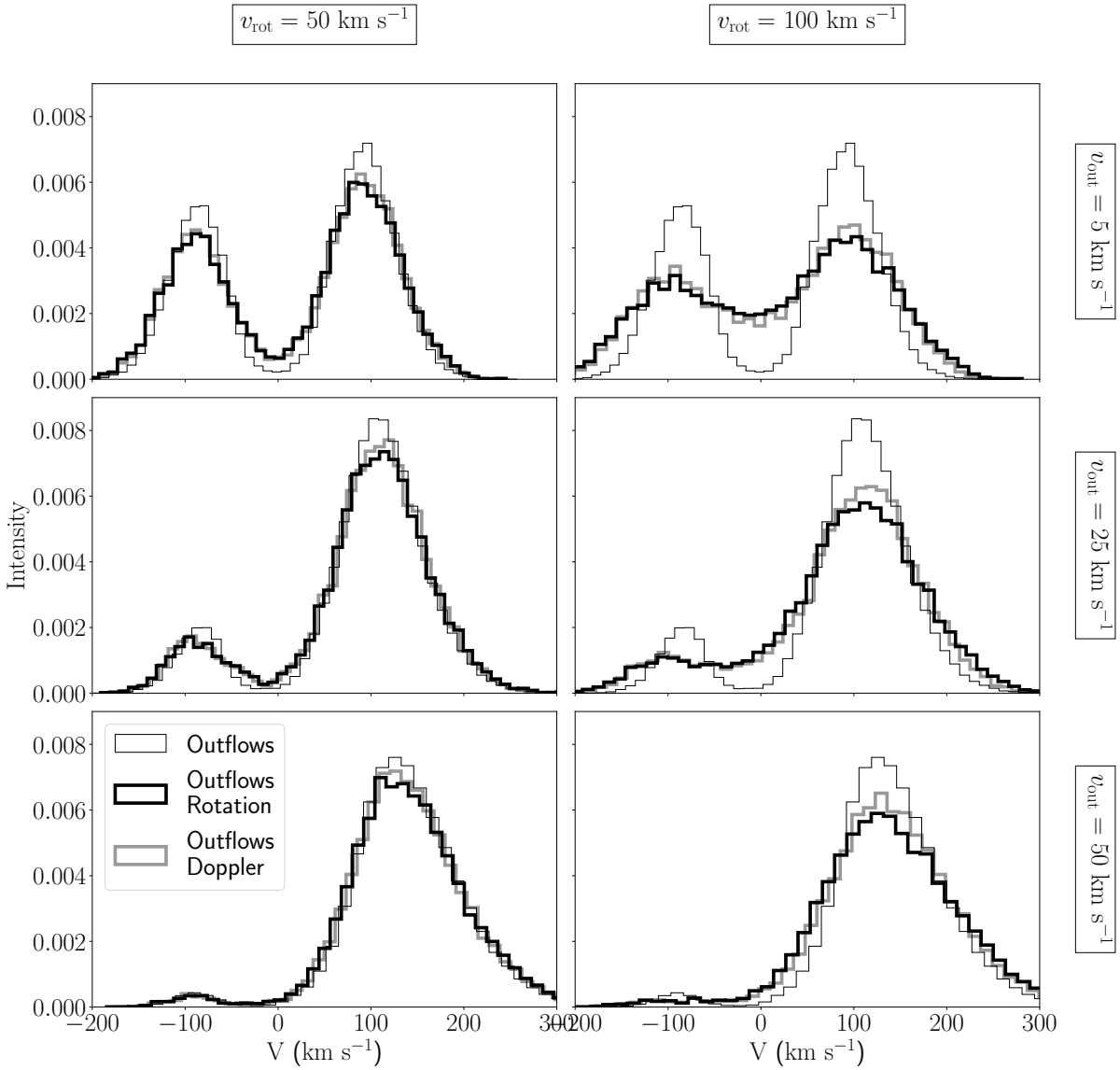

Figure 1. Qualitative trends of changing outflow and rotational velocity viewed perpendicular to the rotation axis. Here we fix $\tau_{\rm H} = 10^6$ and $\theta = 90°$. We vary $V_{\rm rot}$ increasing from left to right and $V_{\rm out}$ increasing from top to bottom. The thin black line corresponds to the Lyα line obtained with CLARA without any rotation and the indicated outflow velocity. The thick black line corresponds to the results including both outflows and rotation. The thick gray line shows the results of modifyin the pure outflow solution by the Doppler shift presented in Equation 4 (in thin line), if there is a radiative transfer of rotation and outflows (thick and clear line), and if there is a radiative transfer of only outflows, but also a Doppler shift from the rotational velocity (thick and dark line).

bottom, and θ according to the legend.

3.3 Doppler Shifts to Include Rotational Effects

In order to compare the line created with the radiative transfer (RT) process that involves the rotation and the line with only outflows that is Doppler shifted (DS), we calculate three main characteristics for each spectrum. We measure the line's standard deviation (STD), skewness (SKW) and bimodality (BI) for both RT's and DS's approaches. We use the definitions in Eqs. 5, 6, 7 for each value (Kokoska & Zwillinger 1999).

$$\mathrm{STD} = \sqrt{m_2}, \tag{5}$$

$$\mathrm{SKW} = \frac{m_3}{m_2^{3/2}}, \tag{6}$$

$$\mathrm{BI} = \mathrm{KURTOSIS} - \mathrm{SKW}^2 = \frac{m_4}{m_2^2} - \frac{m_3^2}{m_2^3}, \tag{7}$$

where each m_i is the i-th moment about the mean. The

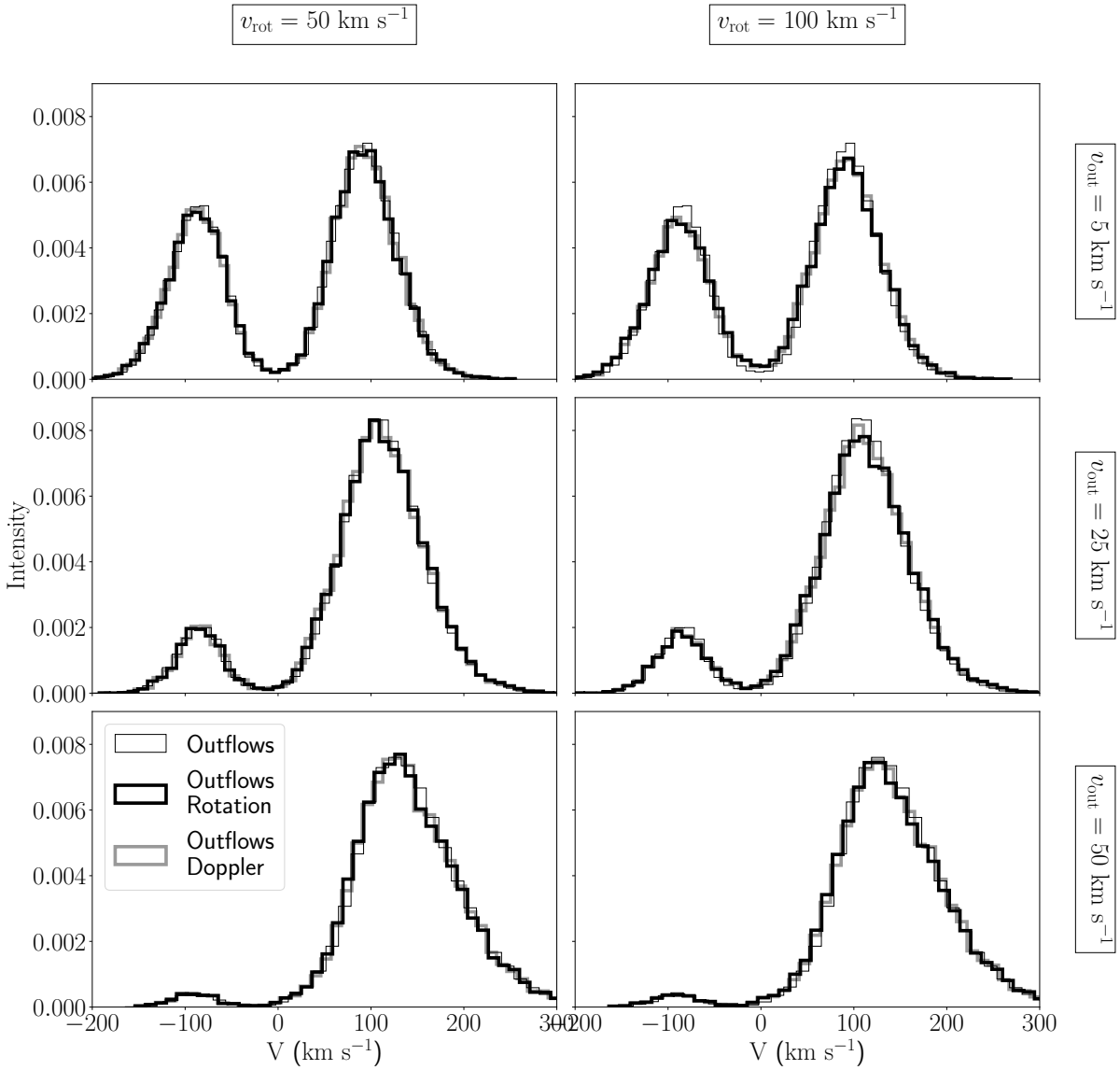

Figure 2. Qualitative trends of changing outflow and rotational velocity viewed parallel to the rotation axis. Here we fix $\tau_{\rm H} = 10^6$ and $\theta = 0°$.

STD has velocity units and quantifies the dispersion of the line's velocity: the larger it is, the wider the line. The SKW is adimensional and quantifies the peaks' asymmetry: if it is > 0 the left peak is taller and if it is < 0 the right peak is taller. The BI is adimensional and quantifies if the line has 1 or 2 peaks: it is always ≥ 1 and the closer it is to 1, the more bimodal is the line (i.e. has 2 peaks).

We plot the results for each value in Figures 3, 4 and 5, respectively for $\tau_{\rm H} = 10^7$. We highlight that these 3 plots increase their fit tendency with a higher optical depth. The reasons why will be discussed in section 4.

This shows that the DS model can reproduce the main characteristics of the RT one. Because of this, we can introduce rotation effects in any spectra without running the radiative transfer simulations, that usually take a significant amount of time and computational resources.

In addition to this, we also evaluate the effects of the viewing angle for fixed rotational and outflows velocity. We measure the intensity of the valley between peaks, for each θ and $\tau_{\rm H}$. Figure 6 summarizes the information with all plots corresponding to the same outflow velocity of $\rm V_{out} = 5$km s^{-1}and rotation velocity of $\rm V_{rot} = 100$km s^{-1}.

4 DISCUSSION

4.1 Theoretical Insights

Why Doppler Shift works. Talk about radiative transfer... In Fig. 7 we present the spectrum of a LAE taken from to different sides of the galaxy. As the LAE is rotating, one side is being redshifted while the other is blueshifted. We see that the combined spectrum is a weighted line, in solid black, that combines these past two. This shows that there

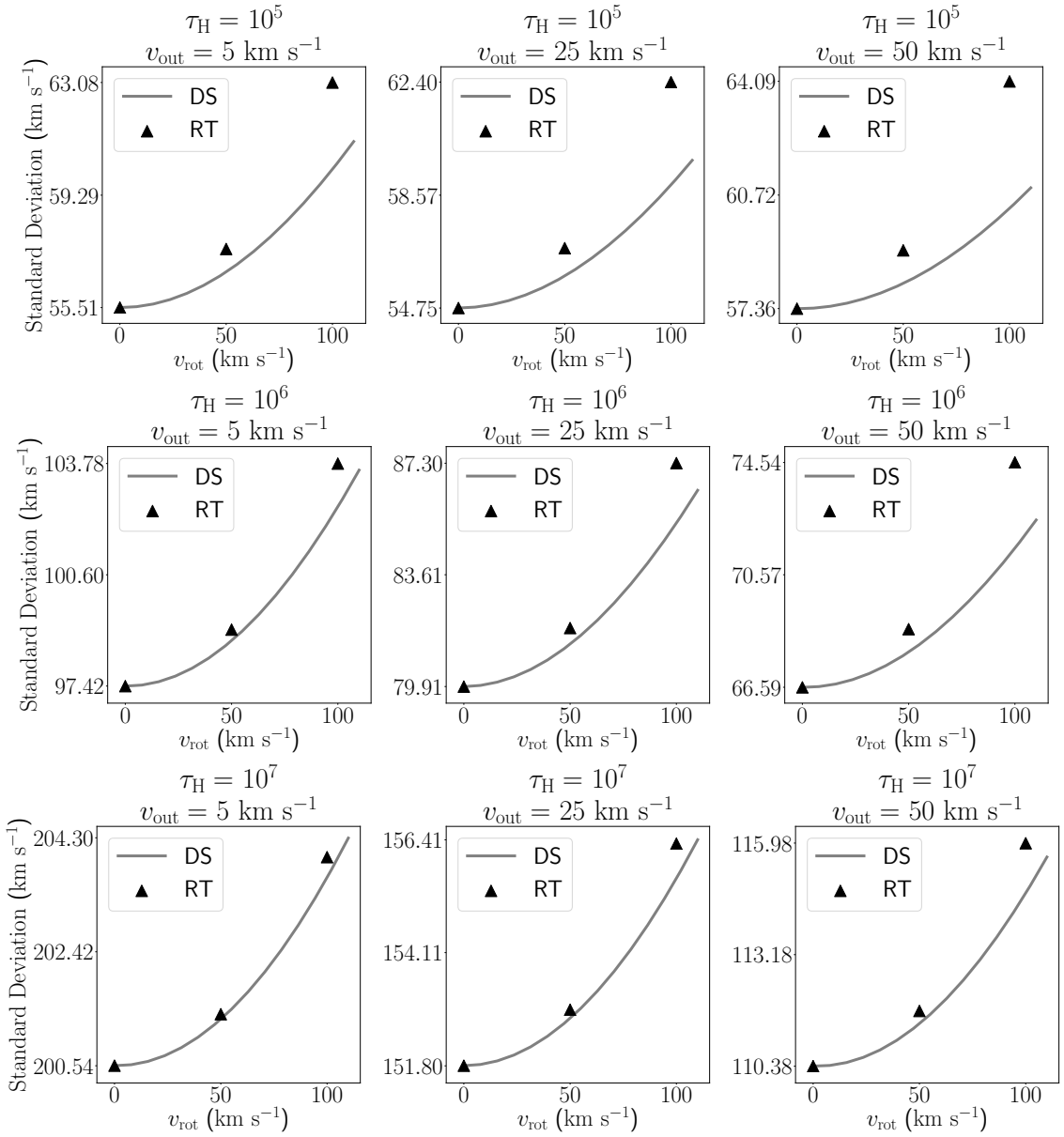

Figure 3. Standard Deviation for RT and DS: The triangles represent the Radiative Transfer and the lines represent the Doppler Shift.

is in fact a Doppler Shift and then it justifies our choice to apply it after the outflows spectrum is obtained.

A first approach to an analytical expression that returns the Lyα spectrum from a rotating galaxy is presented by Garavito-Camargo et al. (2014). This derivation is based on the assumption that the distribution of photons' propagation directions at the edge of the galaxy is anisotropic and depends of τ_H only. So this approximation becomes more accurate with higher optical depth and it is also the reason why the Doppler Shift technique to induce rotational effects to an outflow Lyα spectrum works.

On the other hand, regarding the parameters V_{rot} , V_{out} , and θ for which this model would work, we have the following. The effect of the outflows velocity is much more sensitive on the spectrum than the rotational one; meaning that for a high V_{out} , the V_{rot} value would have to be equal or greater in order to be able to glimpse the shift in frequency that rotation induces. Regarding θ, the introduction of rotation in the model implies that it will only affect galaxies with its viewing angle $\theta \neq 90°$. This can be observed in the cartesian components of the velocity of the atoms (Eq. 1, 2, 3) where the only velocity factor affecting v_z is the outflows one.

4.2 Application to observational data

We find three different approaches how this model can have observational implications. Firstly, as the resolution of astronomical instruments is increasing, new images from LAEs can be spatially resolved in a way that rotation velocities

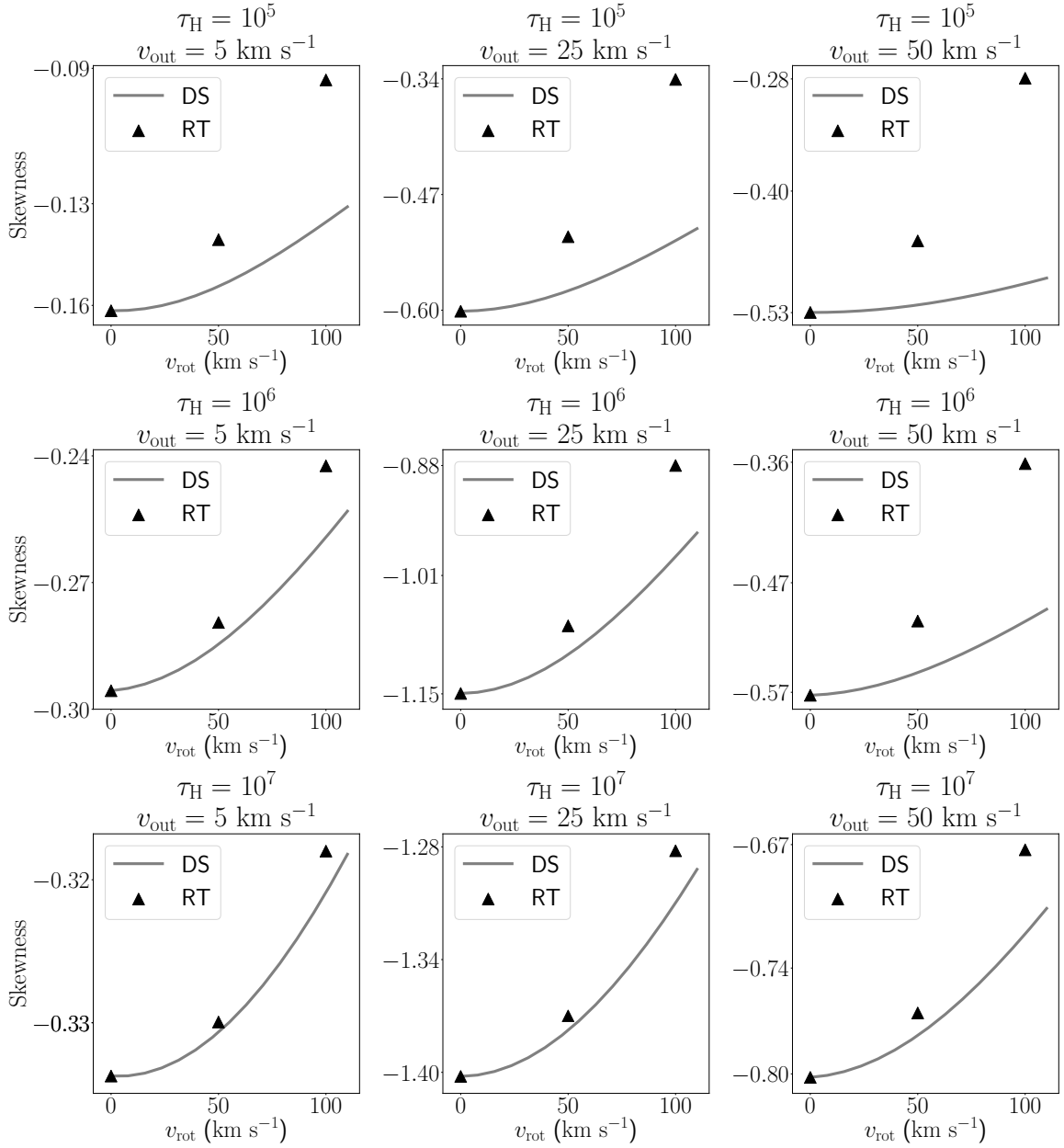

Figure 4. Skewness for RT and DS: The triangles represent the Radiative Transfer and the lines represent the Doppler Shift.

of the galaxy can be determined. New spectrographs like MUSE should help obtain kinematic information from LAEs by using our model. As for now, previous works in the literatures have already found useful data to support this idea. Fig 7 of Prescott et al. Prescott et al. (2015) shows the presence of Doppler shift and Herenz et al. (2016) creates 2D line of sight velocity maps of several LARS (Lyman Alpha Reference Sample) galaxies.

Another application of this new model to the current interpretation of Lyα spectra, is that the central ($V = 0$) emission of the spectra seen in the Lyα line, is a consequence of the viewing angle of the galaxy and can be controlled by it. Several authors have suggested that this central emission is caused by radiation that escapes the galaxy without scattering. So we present an alternative that solves this issue. In addition, the effect of outflows velocities V_{rot} in current models can modify the asymmetry of peaks present in the Lyα line. However the intensity of the valley and the width of the line were not easily reproduced. In this work we provide a tool to provide these effects with values of V_{out} and V_{rot} that do not exceed the typical LAEs' values found in the literature.

Kulas... Finally, we present a reconstruction of a selected Lyα spectrum presented by Kulas et al. (2012) and reproduced with the permission of the author. We create a fit of the Lyα line and predict its kinematic properties.

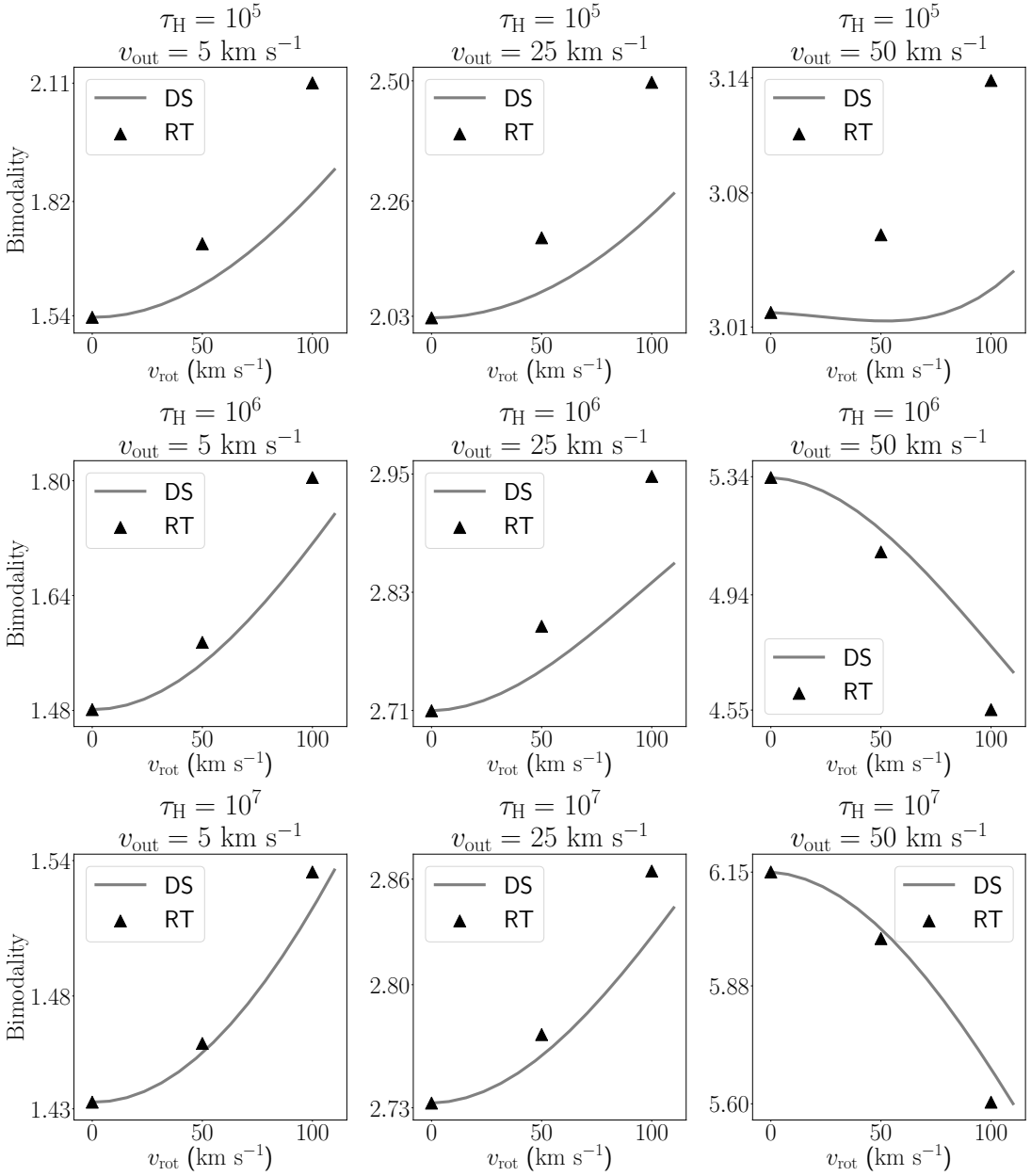

Figure 5. Bimodality for RT and DS: The triangles represent the Radiative Transfer and the lines represent the Doppler Shift.

5 CONCLUSIONS

In this paper we explore, for the first time in the literature, the results of a model for the emergent Lyα line from rotating outflows. The main results for the model are computed from a Monte-Carlo radiative transfer simulation and confronted with a simple semi-analytic ansatz that adds the effects of rotation onto results of pure outflow kinematics.

The main effects of rotation on the Lyα line morphology are:

- Broadening the line.
- Increasing the intensity at the line's center.
- Inducing a dependency on the viewing angle, The closer the observer is to the pole of the galaxy (defined by the rotation axis), the smaller are the effects from rotation.

We found that in the case of solid body rotation these effects can be quantitatively explained by a Doppler boost, where the Doppler factor can be computed as the producet of quantities at the surface of last scattering, namely $\vec{v}_{rot} \cdot \hat{k}$, where $\vec{v}_{rot}$ is the velocity due to rotation and $\hat{k}$ is the direction of the photon's propagation. These conclusions, specially the confirmation of the Doppler boost as a good proxy for solid body rotation, strenghten the evidence reported by Garavito-Camargo et al. (2014) when they modeled the effect of pure rotation on Lyα spectra.

As an application to observational data we find that recent results that take the spectra of two different sides of a galaxy can detect the effect of approaching/receeding gas motions. However, the distances between the peaks of these

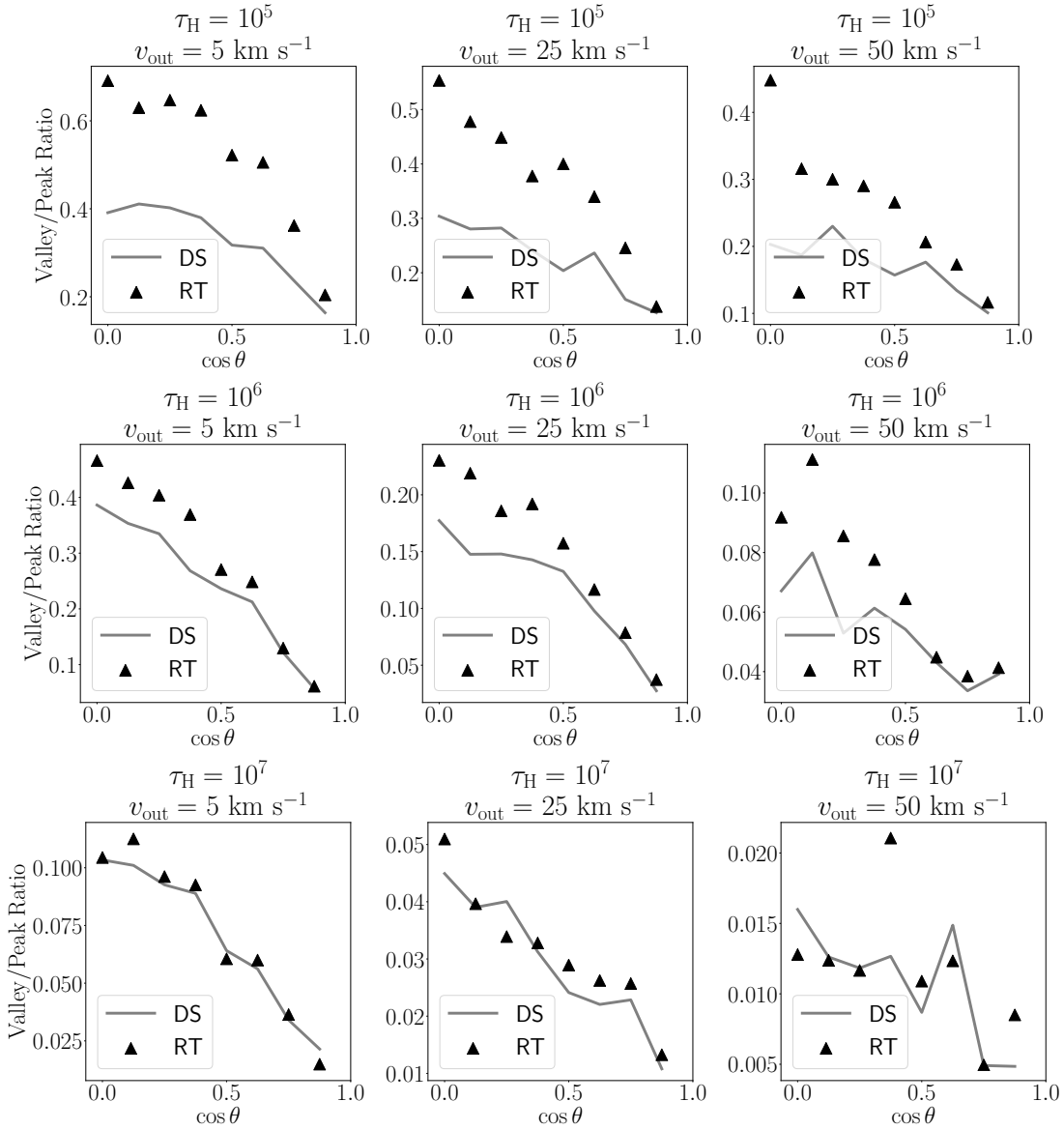

Figure 6. Valley Intensity: We show for each τ_H the dependency that the viewing angle θ has on the line's the valley intensity. The larger $\cos\theta$ the lower is the valley intensity, so the higher θ, the higher the valley intensity. Also, the higher τ_H , the better is the fit RT-DS. We fixed $V_{rot} = 100$km s^{-1}.

two spectra correspond to $\approx v_{rot}\cos\theta$ due to the weights of the emitting regions.

REFERENCES

Ahn S.-H., Lee H.-W., Lee H. M., 2003, MNRAS, 340, 863
Cairós L. M., González-Pérez J. N., 2017, A&A, 600, A125
Cairós L. M., Caon N., Weilbacher P. M., 2015, A&A, 577, A21
Dijkstra M., Haiman Z., Spaans M., 2006, ApJ, 649, 14
Forero-Romero J. E., Yepes G., Gottlöber S., Knollmann S. R., Cuesta A. J., Prada F., 2011, MNRAS, 415, 3666
Garavito-Camargo J. N., Forero-Romero J. E., Dijkstra M., 2014, ApJ, 795, 120
Herenz E. C., et al., 2016, A&A, 587, A78
Kokoska S., Zwillinger D., 1999, CRC standard probability and statistics tables and formulae. Crc Press
Kulas K. R., Shapley A. E., Kollmeier J. A., Zheng Z., Steidel C. C., Hainline K. N., 2012, ApJ, 745, 33
Orsi A., Lacey C. G., Baugh C. M., 2012, MNRAS, 425, 87
Partridge R. B., Peebles P. J. E., 1967, ApJ, 147, 868
Prescott M. K. M., Martin C. L., Dey A., 2015, ApJ, 799, 62
Swaters R. A., Sancisi R., van Albada T. S., van der Hulst J. M., 2009, A&A, 493, 871
Verhamme A., Schaerer D., Maselli A., 2006, A&A, 460, 397

APPENDIX A: ADDITIONAL FIGURES

In this appendix we show Lyα spectra with fixed V_{out} (Fig. A1) and fixed V_{rot} (Fig. A2). For a larger set of spectra with the same fixed V_{out} and V_{rot} refer to Fig. A3 and Fig. A4 respectively.

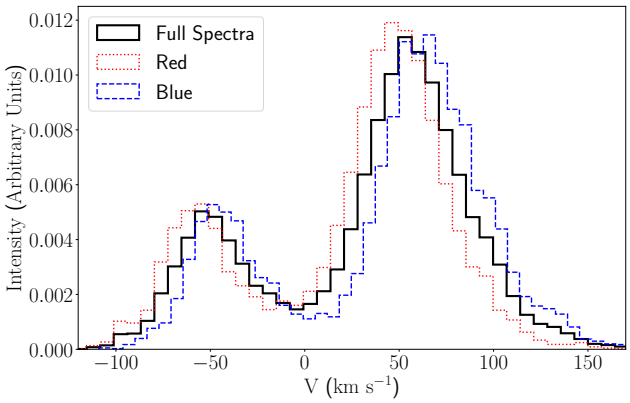

Figure 7. Doppler Shift: We fix V_{out} = 25km s^{-1}, V_{rot} = 100km s^{-1}, $\tau_H = 10^5$.

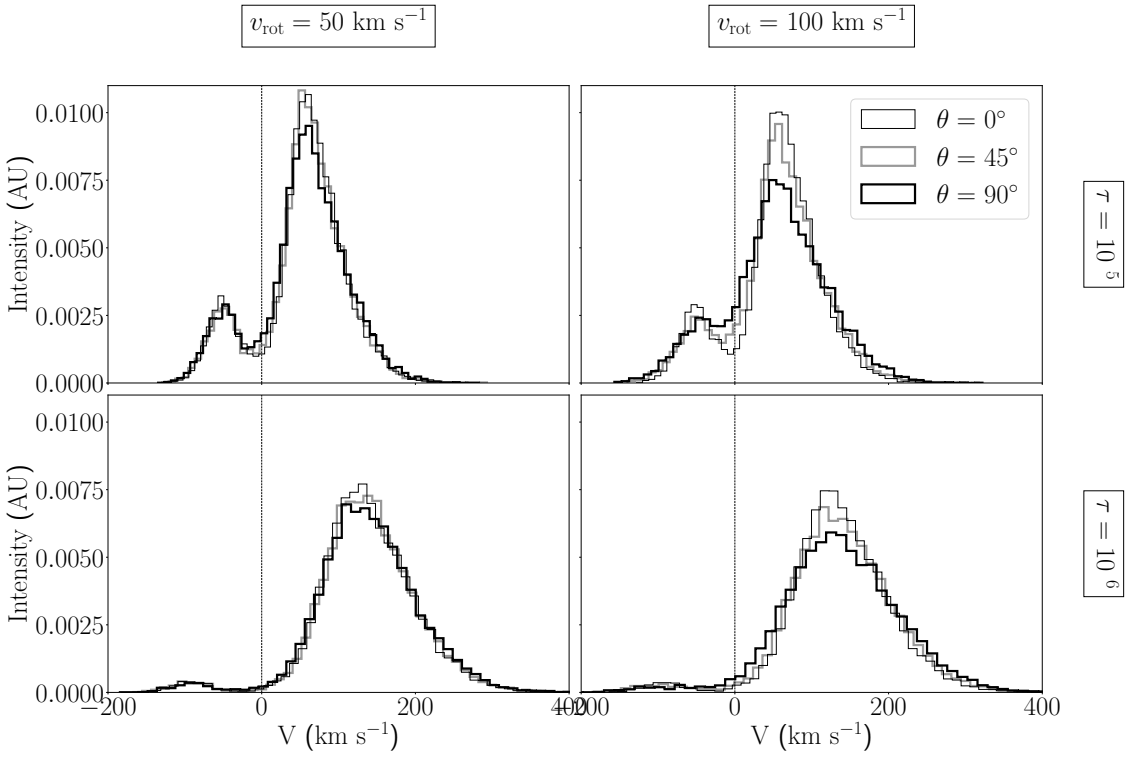

Figure A1. Spectra with fixed outflows velocity: We fix $V_{out} = 50$km s^{-1}.

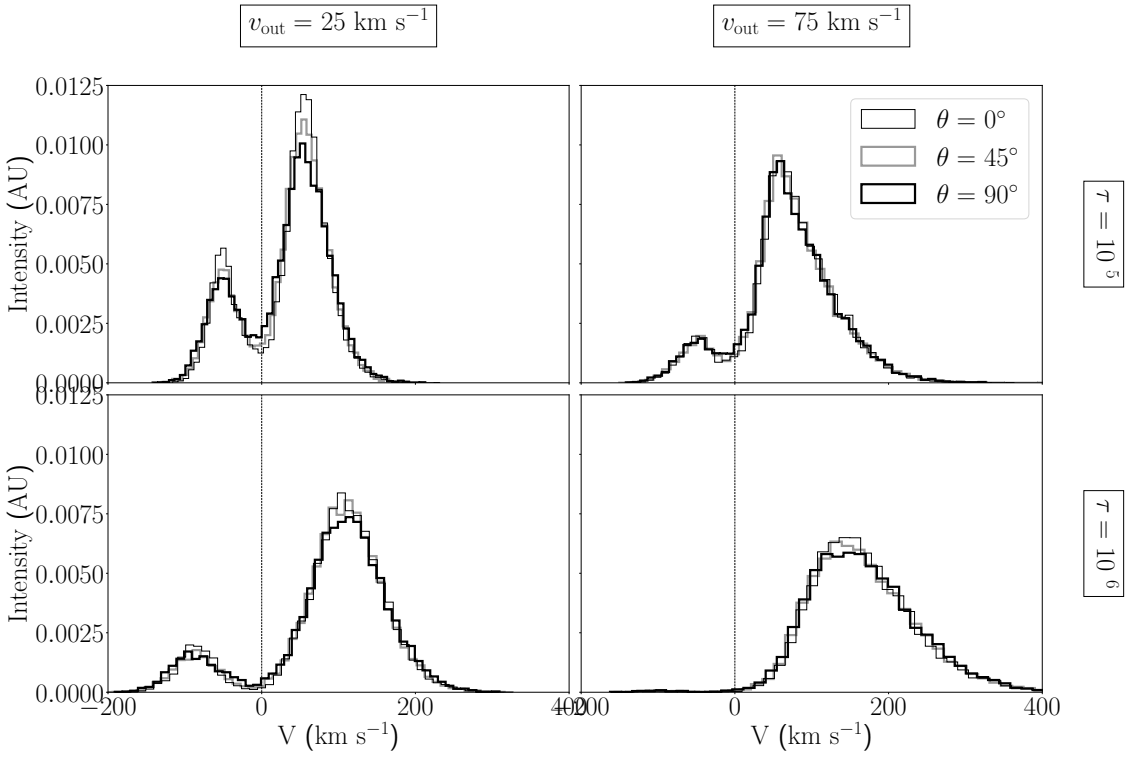

Figure A2. Spectra with fixed rotation velocity: We fix $V_{rot} = 50$km s^{-1}.

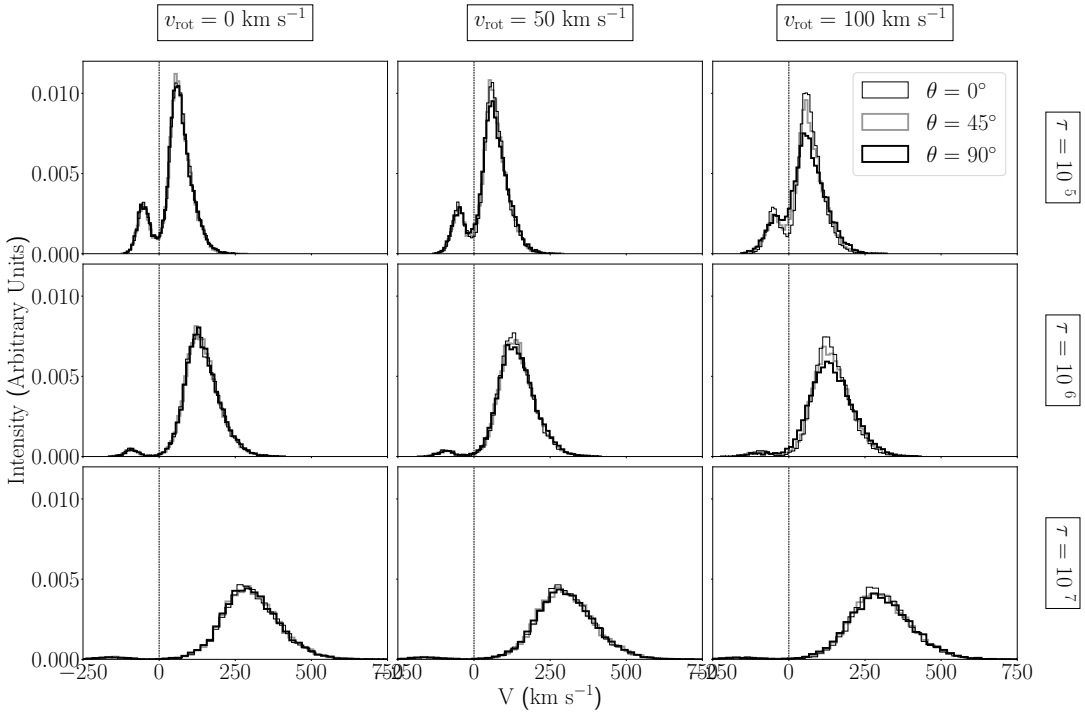

Figure A3. Spectra with fixed outflows velocity: We fix $\rm V_{out} = 50 km\ s^{-1}$.

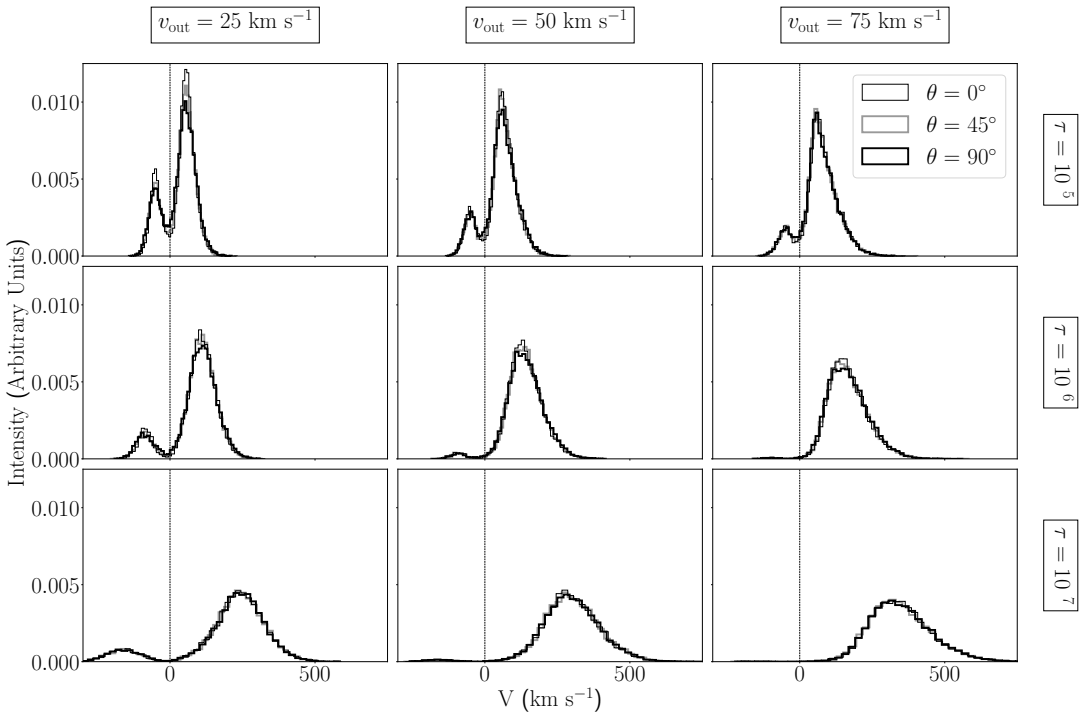

Figure A4. Spectra with fixed rotation velocity: We fix $\rm V_{rot} = 50 km\ s^{-1}$.